The Astrophysical Journal, 836:82 (16pp), 2017 February 10 doi:10.3847/1538-4357/836/1/82

Multiwavelength Transit Observations of the Candidate Disintegrating Planetesimals Orbiting WD 1145+017

Bryce Croll[1], Paul A. Dalba[2], Andrew Vanderburg[3], Jason Eastman[3], Saul Rappaport[4], John DeVore[5], Allyson Bieryla[3], Philip S. Muirhead[1,2], Eunkyu Han[2], David W. Latham[3], Thomas G. Beatty[6], Robert A. Wittenmyer[7], Jason T. Wright[6,8], John Asher Johnson[3], and Nate McCrady[9]

[1] Institute for Astrophysical Research, Boston University, 725 Commonwealth Avenue, Room 506, Boston, MA 02215, USA; brycecroll@gmail.com
[2] Department of Astronomy, Boston University, 725 Commonwealth Avenue, Boston, MA 02215, USA
[3] Harvard-Smithsonian Center for Astrophysics, 60 Garden Street, Cambridge, MA 02138, USA
[4] Kavli Institute for Astrophysics and Space Research, Massachusetts Institute of Technology, Cambridge, MA 02139, USA
[5] Visidyne, Inc., Santa Barbara, CA 93105, USA
[6] Department of Astronomy and Astrophysics and Center for Exoplanets and Habitable Worlds, The Pennsylvania State University, University Park, PA 16802, USA
[7] School of Physics and Australian Centre for Astrobiology, UNSW Australia, Sydney, NSW 2052, Australia
[8] NASA Nexus for Exoplanet System Science
[9] Department of Physics and Astronomy, University of Montana, 32 Campus Drive, No. 1080, Missoula, MT 59812, USA
Received 2015 October 7; revised 2016 December 18; accepted 2016 December 19; published 2017 February 9

Abstract

We present multiwavelength, ground-based follow-up photometry of the white dwarf WD 1145+017, which has recently been suggested to be orbited by up to six or more short-period, low-mass, disintegrating planetesimals. We detect nine significant dips in flux of between 10% and 30% of the stellar flux in our ∼32 hr of photometry, suggesting that WD 1145+017 is indeed being orbited by multiple, short-period objects. Through fits to the asymmetric transits that we observe, we confirm that the transit egress is usually longer than the ingress, and that the transit duration is longer than expected for a solid body at these short periods, all suggesting that these objects have cometary tails streaming behind them. The precise orbital periods of the planetesimals are unclear, but at least one object, and likely more, have orbital periods of ∼4.5 hr. We are otherwise unable to confirm the specific periods that have been reported, bringing into question the long-term stability of these periods. Our high-precision photometry also displays low-amplitude variations, suggesting that dusty material is consistently passing in front of the white dwarf, either from discarded material from these disintegrating planetesimals or from the detected dusty debris disk. We compare the transit depths in the V- and R-bands of our multiwavelength photometry, and find no significant difference; therefore, for likely compositions, the radius of single-size particles in the cometary tails streaming behind the planetesimals must be ∼0.15 μm or larger, or ∼0.06 μm or smaller, with 2σ confidence.

Key words: eclipses – planetary systems – stars: individual (WD 1145+017) – techniques: photometric

1. Introduction

The white dwarf WD 1145+017 was recently announced to host up to six or more disintegrating candidate planetesimals in extremely short-period orbits: Vanderburg et al. (2015) presented two-wheeled *Kepler Space Telescope* (*K2*) photometry (Howell et al. 2014) of WD 1145+017 with six distinct occultations with periods from ∼4.5–4.9 hr and depths up to a few percent. The depth of the main ∼4.5 hr transiting object also evolved from undetectable to a few percent over the 80 days of long cadence *K2* photometry. As the long cadence (∼29.4 minutes) *Kepler* integrations were poorly suited to resolve what likely should be events with very short transit durations (∼1 minute) at these ultra-short periods, follow-up photometry was performed: Vanderburg et al. (2015) detected ∼40% eclipses with an asymmetric transit profile using the 1.2 m Fred L. Whipple Observatory, and the MEarth South array of 0.4 m telescopes (Nutzmann & Charbonneau 2008; Irwin et al. 2015). These observed apparent occultations of WD 1145+017 displayed many characteristics in common with other candidate disintegrating, ultra-short period planets, including variable transit depths, and an asymmetric transit profile featuring a sharp ingress and gradual egress; in this case—and in the case of the three other ultra short-period, low-mass, disintegrating planet candidates that have been claimed to date (KIC 12557548; Rappaport et al. 2012, KOI-2700b; Rappaport et al. 2014, and K2-22b; Sanchis-Ojeda et al. 2015)—these characteristics are interpreted as being due to a variable amount of material disintegrating from the planets/planetesimals that condenses at altitude into a dusty cometary tail streaming behind the planets/planetesimals.

That WD 1145+017 might be the best example of a white dwarf orbited by close-in planets/planetesimals is strengthened by two additional lines of evidence: the spectrum of WD 1145+017 is significantly polluted, and it displays an infrared excess. A visible spectrum of WD 1145+017 revealed spectral lines of calcium, aluminum, magnesium, silicon, nickel, and iron (Vanderburg et al. 2015); as the settling time of these elements is rapid (∼1 million years) compared with the age of this white dwarf (∼175 million years), these elements must have recently accreted onto the white dwarf. Vanderburg et al. (2015) also found evidence for an infrared excess likely arising from a ∼1150 K warm dusty debris disk; such a debris disk could be the source of the planetesimals that have been observed to pass in front of this white dwarf.

WD 1145+017 is arguably the most compelling example of the many white dwarfs that have been observed to be significantly polluted as a result of what has been claimed to be the accretion of rocky bodies. Approximately 1/3 of all white dwarfs cooler than 20,000 K display the presence of elements heavier than hydrogen/helium (Zuckerman et al. 2003, 2010; Koester et al. 2014); for white dwarfs of

Table 1
Observing Log

Date (UTC)	Telescope and Instrument	Observing Band	Duration (hr)	Exposure Time (s)	Overhead[a] (s)	Airmass	Conditions	Aperture[b] (pixels)
2015 May 08	Perkins/PRISM	V	3.85	45	6.3	1.21 → 1.20 → 1.98	Occasional clouds	8, 16, 24
2015 May 08	FLWO/KeplerCam	V	1.77	60	16.0	1.16 → 1.30	Occasional clouds	8, 20, 32
2015 May 09	MINERVA T1	R	3.88	60	6.0	1.16 → 2.19	Clear	8, 20, 32
2015 May 09	MINERVA T3	air	3.77	60	6.0	1.16 → 2.22	Clear	8, 20, 32
2015 May 09	MINERVA T4	air	4.50	60	6.0	1.18 → 1.16 → 1.99	Clear	8, 20, 32
2015 May 10	MINERVA T1	R	5.15	60	6.0	1.16 → 5.81	Clear	8, 20, 32
2015 May 10	MINERVA T2	V	4.91	60	6.0	1.16 → 4.86	Clear	8, 20, 32
2015 May 10	MINERVA T3	air	4.46	60	6.0	1.20 → 7.91	Clear	8, 20, 32
2015 May 10	MINERVA T4	air	2.79	60	6.0	1.52 → 7.94	Clear	8, 20, 32
2015 May 11	DCT/LMI	V	3.40	30	8.6	1.48 → 1.03	Clear	13, 25, 35
2015 May 11	FLWO/KeplerCam	V	4.53	60	16.0	1.17 → 1.16 → 2.17	Clear	8, 20, 32
2015 May 11	MINERVA T1	R	2.17	60	6.0	1.24 → 1.92	Clear	8, 20, 32
2015 May 11	MINERVA T2	V	4.17	60	6.0	1.17 → 1.16 → 1.91	Clear	8, 20, 32
2015 May 11	MINERVA T3	air	4.24	60	6.0	1.18 → 1.16 → 1.92	Clear	8, 20, 32
2015 May 11	MINERVA T4	air	4.21	60	6.0	1.17 → 1.16 → 1.92	Clear	8, 20, 32
2015 May 12	Perkins/PRISM	R	3.96	45	6.0	1.21 → 1.20 → 1.97	Clear	8, 16, 24
2015 May 12	MINERVA T1	V	3.99	60	6.0	1.16 → 1.91	Occasional clouds	8, 20, 32
2015 May 12	MINERVA T2	V	4.15	60	6.0	1.17 → 1.16 → 1.91	Occasional clouds	8, 20, 32
2015 May 12	MINERVA T3	air	3.99	60	6.0	1.16 → 1.90	Occasional clouds	8, 20, 32
2015 May 12	MINERVA T4	air	4.15	60	6.0	1.17 → 1.16 → 1.91	Occasional clouds	8, 20, 32
2015 May 13	Perkins/PRISM	V	2.34	45	6.5	1.26 → 1.97	Thin clouds to clear	8, 16, 24
2015 May 13	MINERVA T1	R	1.56	60	6.0	1.34 → 1.94	Occasional clouds	8, 20, 32
2015 May 13	MINERVA T2	B	4.13	60	6.0	1.17 → 1.16 → 1.95	Occasional clouds	8, 20, 32
2015 May 13	MINERVA T4	air	4.13	60	6.0	1.16 → 1.95	Occasional clouds	8, 20, 32
2015 May 18	DCT/LMI	R	0.96	30	8.5	1.27 → 1.43	Clear	10, 20, 30
2015 May 18	MINERVA T1	R	3.20	60	6.0	1.16 → 1.88	Clear	8, 20, 32
2015 May 18	MINERVA T2	B	3.72	60	6.0	1.16 → 1.93	Clear	8, 20, 32
2015 May 18	MINERVA T4	air	3.71	60	6.0	1.16 → 1.93	Clear	8, 20, 32
2015 May 22	Perkins/PRISM	R	2.79	45	6.0	1.22 → 1.90	Clear	8, 16, 24
2015 May 23	Perkins/PRISM	R	2.15	45	7.0	1.22 → 1.59	Occasional clouds	8, 16, 24

Notes.
[a] The overhead includes time for read-out, and any other applicable overheads.
[b] We give the radius of the aperture, the radius of the inner annulus and the radius of the outer annulus that we use for sky subtraction in pixels.

these temperatures, elements heavier than hydrogen and helium sink beneath the outer layers quickly compared to the cooling time. Although it was originally suggested that this material originated from the interstellar medium (e.g., Dupuis et al. 1993), the currently accepted, canonical origin for these elements is that they resulted from material from asteroids or more massive rocky bodies that have been orbitally perturbed (Debes & Sigurdsson 2002), are tidally disrupted—often into a debris disk—and then material from these bodies gradually or quickly accretes onto the white dwarf (Jura 2003; Zuckerman et al. 2010). The reason that the origin of these polluting elements is thought to result from rocky bodies is that analyses of high-resolution spectra of polluted white dwarfs have allowed the elemental abundances of these polluting materials to be measured, and they are broadly consistent with rocky, terrestrial solar system bodies with refractory-rich and volatile-poor material[10] (e.g., Zuckerman et al. 2007; Dufour et al. 2010; Klein et al. 2010).

One method of lending credence to the disintegrating planet/planetesimal candidate scenario is through multiwavelength observations to constrain the particle size of the dusty material in the cometary tails trailing these objects. This has already been attempted for the candidate disintegrating planet KIC 12557548b; optical and near-infrared observations of two transits of KIC 12557548b suggested that the grain sizes trailing KIC 12557548b were $\sim$0.5 μm in radius or larger (Croll et al. 2014), while optical multiwavelength observations suggested the particle sizes were 0.25–1.0 μm (Bochinski et al. 2015). Multiwavelength optical photometry of one transit of the disintegrating low-mass candidate exoplanet K2-22b suggests approximate particle sizes of 0.2–0.4 μm in the cometary tail trailing that body (Sanchis-Ojeda et al. 2015).

For the candidate planetesimals orbiting WD 1145+017, multiwavelength observations may help determine the mechanism that generates the dust that is believed to be trailing these objects. The preferred explanation of Vanderburg et al. (2015) for the apparent dusty tails was that the high temperatures of these planetesimals in these short-period orbits would result in material sublimating off the planetesimals' surfaces with sufficient thermal speed to overcome the escape speed on these low surface gravity objects; at altitude these vapors would condense into dust. For the other disintegrating, planet-mass candidates, vapor is believed to be driven from the higher surface gravity of these planets by a Parker-wind, before similarly condensing into dust at altitude (Rappaport et al. 2012, 2014; Perez-Becker & Chiang 2013; Sanchis-Ojeda et al. 2015). In these other disintegrating systems, the

[10] Although there have now been a few polluted white dwarfs with spectra that are believed to result from volatile/water-rich asteroids (e.g., Farihi et al. 2013; Raddi et al. 2015).

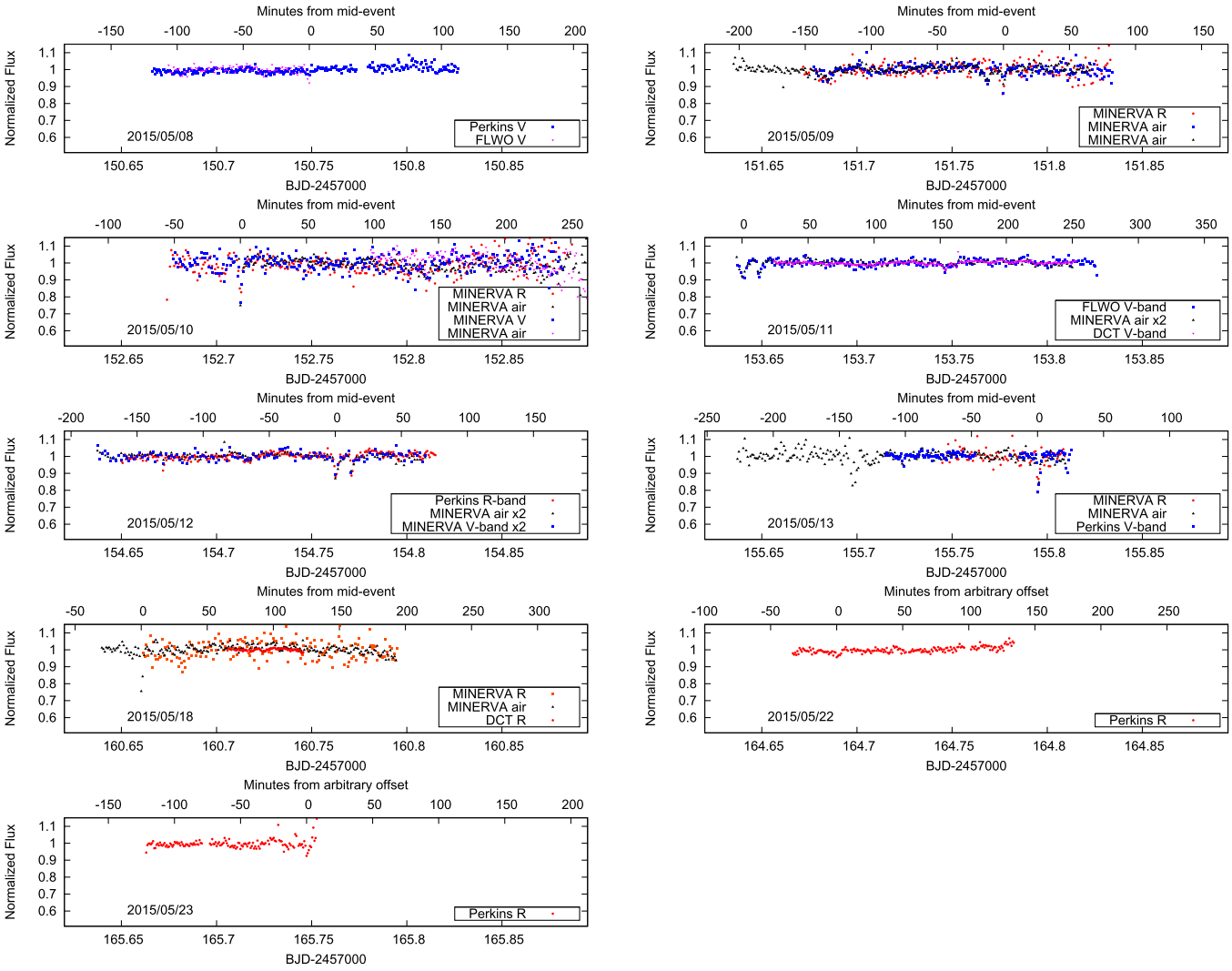

Figure 1. Perkins/PRISM, DCT/LMI, FLWO/KeplerCam, and MINERVA photometric observations of WD 1145+017. The UTC date of observations are given in the lower-left of each panel, while the telescope and band of observations are given in the legend at the lower-right. The minutes from mid-event for each night of observations are given from the deepest decrement in flux observed in each night, if this decrement in flux is believed to be statistically significant. For the "MINERVA air x2" and "MINERVA V-band x2" data, observations of two MINERVA telescopes in the "air" and V-bands respectively, have been combined using their weighted mean.

presumed higher planet masses of these candidates, and therefore the higher surface gravities, require a Parker-wind, compared to the assumed Ceres-mass planetesimals of the WD 1145+017 system, where the lower surface gravities allow material to freely stream from the planetesimals. Alternative possibilities to explain the dusty material in the cometary tails of the planetesimals in this system include (i) that these bodies could be similar to comets in our own solar system with low enough surface gravities that their dust tails are carried off by the disintegration of volatiles, (ii) that these planetesimals and their cometary tails are the result of collisions with other planetesimals in the system or the observed debris disk, or (iii) that tidal forces from the white dwarf have ripped larger bodies apart, or are in the process of ripping apart such bodies, and we are observing the tidally disrupted bodies that have possibly formed the observed debris disk. The rigid-body Roche limit for a Ceres-density asteroid around this white dwarf (using the assumed white-dwarf mass of 0.6 $M_{\odot}$; Vanderburg et al. 2015) is at an orbital period of ∼3.4 hr, suggesting that if these planetesimals are similar to the asteroids in our own solar system they should already be subjected to considerable tidal forces that may be threatening to rip them apart. In the latter two cases of a collision or a tidally disrupted body, shear would likely quickly result in material trailing behind the planetesimals (Veras et al. 2014), forming cometary tails. Naively, a tidally disrupted body would suggest larger particle sizes in the trailing tails, if they are similar to disrupted bodies in our own solar system (e.g., Michikami et al. 2008; Jewitt et al. 2010, 2013).

Here we report a wealth of multiwavelength follow-up photometry of WD 1145+017 that considerably strengthens the conclusion that this star is being orbited by a number of low-mass bodies with dusty trails trailing behind them. We present multiwavelength ground-based photometry from a variety of telescopes in Section 2; we display a number of significant decrements in flux of up to ∼30% of the stellar flux, likely the result of planetesimals with dusty tails passing in front of the white dwarf host and scattering light out of the line of sight. We analyze the depths, duration, and timing of these eclipses in Section 3; the egress timescale of these transits is usually longer than the ingress timescale, and the transit duration is longer than we would expect for a circular orbit of

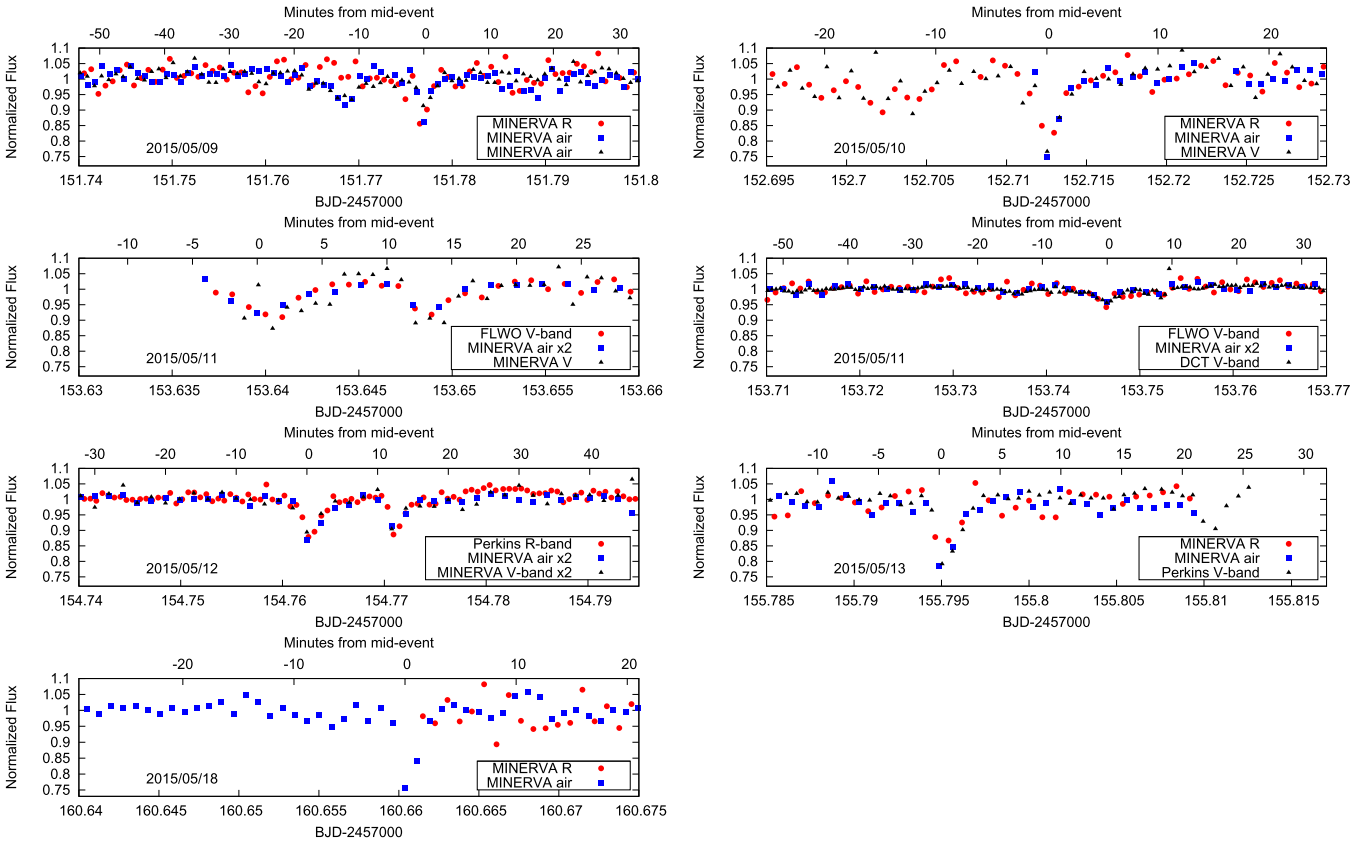

Figure 2. DCT, Perkins, FLWO, and MINERVA multiwavelength photometry of WD 1145+017, zoomed-in on durations when significant decrements in flux are observed. The UTC dates of observations are given in the lower-left of each panel, while the telescope and band of observations are given in the legend at the lower-right. For the "MINERVA air x2" and "MINERVA V-band x2" data, observations of two MINERVA telescopes in the "air" and V-bands respectively, have been combined using their weighted mean. The minutes from mid-event are given from the deepest decrement in flux observed in each panel.

an Earth-sized body at these short periods, findings that are both consistent with the hypothesis that this system contains short-period planetesimals trailed by dusty, cometary tails. The exact periods of these planetesimals are uncertain, but several objects appear to have periods of approximately ∼4.5 hr; with this many objects with nearly identical periods it is unclear whether the orbits of these objects are stable. Lastly, the ratio of the transit depths from our multiwavelength V and R-band observations allow us to conclude that if the dust grains trailing the planetesimals in the WD 1145+017 system are all of a single size then they have a radius of ∼0.15 μm or larger, or ∼0.06 μm or smaller, with 2σ confidence.

2. Observations

We observed WD 1145+017 on a variety of nights in 2015 May with a number of different ground-based telescopes. These include the Discovery Channel Telescope (DCT) and its Large Monolithic Imager (LMI; Massey et al. 2013), the Perkins 1.8 m telescope and its PRISM imager (Janes et al. 2004), the Fred L. Whipple Observatory 1.2 m telescope and its KeplerCam imager (Szentgyorgyi et al. 2005), and the four MINERVA 0.7 m robotic telescopes, labeled T1-T4 (Swift et al. 2015). We summarize these observations in Table 1. For the DCT/LMI observations, we utilized 4-amplifier read-out and 2 × 2 pixel binning to improve the duty-cycle. The DCT/LMI, Perkins/PRISM and MINERVA data are processed by dark/bias subtracting the data, and then we divide through by a sky-flat. The FLWO/KeplerCam data are processed using the techniques discussed in Carter et al. (2011). Aperture photometry is performed using the techniques discussed in Croll et al. (2015) and references therein; the aperture radii, and the radii of the inner and outer annuli we use to subtract the sky are given in Table 1. The filters used on the various telescopes were: the DCT/LMI observations utilized an Andover V-band filter and a Kron Cousins R-band filter, the FLWO/KeplerCam observations utilized a Harris V-filter, the MINERVA observations utilized Johnson B, V and R-band filters, while the the Perkins/PRISM observations utilized Johnson V and R-band filters. The MINERVA "air"-band observations are simply those conducted without a filter, and therefore the wavelength dependence is given by the quantum efficiency of the MINERVA CCDs (Swift et al. 2015); the MINERVA CCDs are quantum efficient across a wide wavelength range—from near-ultraviolet to near-infrared wavelengths—with central wavelengths of: ∼0.64 μm for the MINERVA T1 and T4 telescopes, and ∼0.71 μm for the MINERVA T3 telescope.[11]

As our observations indicate that WD 1145+017 displays low level variability, likely due to dusty material passing consistently in front of the star (see Section 3.5), to estimate the errors on our photometry we cannot take the root mean square of the differential photometry of WD 1145+017; instead we take the mean of the root mean square of the differential photometry of nearby reference stars that have similar aperture flux values as WD 1145+017 (we take the mean of the root mean square of the differential photometry of all stars, that are

[11] The MINERVA T2 telescope observed only in the B and V-bands.

not obvious variables, with aperture flux values within 20% of WD 1145+017). All the Julian dates have been converted to and presented as barycentric Julian dates using the terrestrial time standard (Eastman et al. 2010).

We present our DCT, Perkins, FLWO, and MINERVA observations in Figure 1. We observe occasional significant decrements in flux of up to ~30% that we interpret as objects, likely with dusty tails streaming behind them, passing in front of the white dwarf along our line of sight. We present our multi-telescope, and often multiwavelength, observations of these significant flux decrements in Figure 2.

3. Analysis

For our light curves where a significant flux decrement is observed we fit the apparent asymmetric transit dips with an "asymmetric hyperbolic secant," which has been applied previously to fit the transit profile of the candidate disintegrating low-mass planet KOI-2700b (Rappaport et al. 2014). As the periods of the planetesimals around WD 1145+017 are not well defined, we replace the explicit reference to phase with that of the time, t, in the asymmetric hyperbolic secant expression of Rappaport et al. (2014); therefore the profile we fit our transits with has a flux, F, at time, t, of:

$$F(t) = F_0 - C\left[e^{-(t-\tau_0)/\tau_1} + e^{(t-\tau_0)/\tau_2}\right]^{-1} \quad (1)$$

F_0 is the out-of-transit flux, $C/2$ is approximately the transit depth as indicated in Equation (2), τ_0 is approximately the transit mid-point, and τ_1 and τ_2 are the characteristic durations of the ingress and egress, respectively. The minimum of the function has a depth—which we will refer to as the transit depth, D—given by:

$$D = \frac{C\xi^{\xi/(1+\xi)}}{1+\xi} \quad (2)$$

and occurs at a time $T_{\rm min}$ of:

$$T_{\rm min} = \tau_0 + \frac{\tau_1\tau_2 \ln(\tau_2/\tau_1)}{\tau_1+\tau_2} \quad (3)$$

where $\xi = \tau_2/\tau_1$.

For those transits that we observe with a single telescope we fit these light curves individually using Equation (1); the results are given at the bottom of Table 2 and are presented in Figure 3. For the transits where we are able to obtain multi-telescope coverage, and usually multiwavelength coverage, we fit F_0 and C individually for each light curve, while fitting τ_0, τ_1 and τ_2 jointly. The results for the joint fits are given at the top of Table 2 and are presented in Figure 4. We quote D and $T_{\rm min}$, rather than C and τ_0, in Table 2. We use Markov Chain Monte Carlo (MCMC) fitting, as described for our purposes in Croll (2006). As a metric of the goodness-of-fit we also quote the reduced χ^2 (χ^2_R) in Table 2; occasionally we observe large χ^2_R values, and in some cases we believe this may be evidence for low-level variability of WD 1145+017, which we discuss in detail in Section 3.5. When multiple apparent dips are observed in a single evening of observations, we differentiate between these different transits using a letter label; we label the first transit of the evening with "A," the next with "B," and so-on. We note that we bin our asymmetric hyperbolic secant model to account for the finite exposure times when comparing with our photometry during our fitting process.

We also fit the ~40% occultations of WD 1145+017 that were detected with the FLWO and MEarth telescopes that were published in Vanderburg et al. (2015); we also confirm two other events that were listed as possible events in Vanderburg et al. (2015), including an additional ~25% event observed with the FLWO on 2015 March 22, and a ~15% event observed on 2015 April 18 with the MEarth and MINERVA/T3 telescopes. The MEarth data are reduced and photometry is produced as outlined in Vanderburg et al. (2015), while the FLWO and MINERVA/T3 data are reduced as discussed in Section 2. The MINERVA/T3 data on 2015 April 18 (UTC) were obtained with the altitude–azimuth derotator not functioning, and therefore suffer from systematics that are most apparent after the drop in flux that we interpret as a transit that evening; we therefore, conservatively, artificially scale up the errors on these points to 10%, and do not use this transit for transit depth comparisons. The fits to the Vanderburg et al. (2015) photometry are presented in Figures 5 and 6, and are given in Table 2.

Lastly, we summarize the ratio of the transit depths, D, we find for our multiwavelength observations in Table 3.

3.1. The Frequency of Significant Transits

In Table 2 we present nine transits with depths, D, greater than ~10% of the stellar flux from our 2015 May photometry. The number of non-overlapping hours of observation from MINERVA, FLWO, the DCT, or the Perkins telescope during the month of 2015 May that would be sensitive[12] to these nine significant transits is ~32 hr; therefore during our observations the frequency of 10% transit dips is ~0.28 per hour, or ~3.6 hr per significant event.

3.2. Transit Duration Changes

We approximate the transit duration by $3 \times (\tau_1 + \tau_2)$; this captures ~94% of the area of the asymmetric hyperbolic secant curve, and appears to qualitatively match the approximate transit duration as indicated by visually inspecting Figures 3–6. The weighted mean of the transit durations we measure is: $3 \times (\tau_1 + \tau_2) = 7.49 \pm 0.15$ minute. In comparison the crossing time of an object with a 4.5–4.9 hr period in a circular orbit around WD 1145+017 should be ~1 minute.

If we assume that all the ground-based eclipses in Table 2 have the same transit duration, the reduced χ^2 of this model is 12.6. Therefore, there may be evidence that the transit duration is not constant for the transits we observe. For instance, the 2015 May 11 "A" transit has an eclipse duration of $3 \times (\tau_1 + \tau_2) = 10.0^{+1.4}_{-1.6}$ minute. We display the transit duration of the eclipses observed from the ground in the top panel of Figure 7.

Our mean transit duration also informs us on the size of the occulting region transiting in front of the white dwarf—in this case the size, or the length, of the candidate planetesimal and the cometary tail streaming behind it. Using the typical equation for the transit duration (Equation (14) of Winn 2010) and assuming a circular, edge-on orbit with a ~4.5 hr period, the stellar radius and mass ($R_* = 1.4\ R_\oplus$; $M_* = 0.6\ M_\odot$) quoted in Vanderburg et al. (2015), and a planetesimal mass much lower than the stellar mass, a transit duration of $3 \times (\tau_1 + \tau_2) \sim 7.49$ minutes is produced by an occulting region of size $R_o \sim 9.5\ R_\oplus$.

[12] To be conservative we exclude ~10 minutes at the start and end of each night of observations, and exclude data with significant cloud cover, or that is otherwise unreliable.

Table 2
Hyperbolic Secant Fits

Date (UTC) and Transit #	Telescope	Band	F_0	D (%)	$T_{\min}$ (JD-2457000)	τ_1 (minute)	τ_2 (minute)	τ_2/τ_1	$3\times(\tau_2+\tau_1)$ (minute)	χ^2_R
				Joint Fits						
2015 May 09	MINERVA/T1	R	$1.005^{+0.009}_{-0.009}$	$14.5^{+3.6}_{-4.0}$	$151.77662^{+0.00017}_{-0.00018}$	$0.20^{+0.10}_{-0.20}$	$1.96^{+0.52}_{-0.73}$	$8.3^{+4.7}_{-7.1}$	$6.5^{+1.6}_{-2.3}$	$5.99^{+0.11}_{-0.15}$
2015 May 09	MINERVA/T3	Air	$1.042^{+0.007}_{-0.008}$	$20.1^{+2.9}_{-3.8}$						
2015 May 09	MINERVA/T4	Air	$1.000^{+0.009}_{-0.009}$	$9.2^{+3.1}_{-3.5}$						
2015 May 10	MINERVA/T1	R	$1.028^{+0.008}_{-0.008}$	$27.7^{+4.5}_{-5.1}$	$152.71259^{+0.00013}_{-0.00011}$	$0.35^{+0.17}_{-0.21}$	$1.08^{+0.27}_{-0.32}$	$3.0^{+1.6}_{-2.3}$	$4.3^{+1.0}_{-1.2}$	$1.94^{+0.05}_{-0.06}$
2015 May 10	MINERVA/T2	V	$1.018^{+0.005}_{-0.005}$	$28.1^{+3.0}_{-3.3}$						
2015 May 10	MINERVA/T3	Air	$1.021^{+0.012}_{-0.012}$	$29.2^{+4.7}_{-5.1}$						
2015 May 11-A	FLWO	V	$1.018^{+0.004}_{-0.005}$	$11.0^{+0.9}_{-0.8}$	$153.64016^{+0.00016}_{-0.00015}$	$1.92^{+0.33}_{-0.38}$	$1.42^{+0.32}_{-0.40}$	$0.7^{+0.2}_{-0.3}$	$10.0^{+1.4}_{-1.6}$	$2.09^{+0.10}_{-0.15}$
2015 May 11-A	MINERVA/T3	Air	$1.026^{+0.005}_{-0.006}$	$10.5^{+1.2}_{-1.2}$						
2015 May 11-A	MINERVA/T4	Air	$0.999^{+0.007}_{-0.007}$	$10.1^{+1.4}_{-1.4}$						
2015 May 11-B	FLWO	V	$1.016^{+0.005}_{-0.005}$	$11.0^{+1.2}_{-1.5}$	$153.64838^{+0.00014}_{-0.00012}$	$0.37^{+0.18}_{-0.16}$	$2.59^{+0.41}_{-0.46}$	$7.0^{+2.5}_{-3.6}$	$8.9^{+1.3}_{-1.5}$	$1.77^{+0.17}_{-0.25}$
2015 May 11-B	MINERVA/T2	V	$1.045^{+0.009}_{-0.010}$	$19.2^{+2.2}_{-2.6}$						
2015 May 11-B	MINERVA/T3 and T4	Air	$1.021^{+0.005}_{-0.005}$	$10.6^{+1.6}_{-1.9}$						
2015 May 11-C	DCT	V	$0.996^{+0.000}_{-0.000}$	$3.8^{+0.1}_{-0.1}$	$153.74646^{+0.00004}_{-0.00004}$	$1.44^{+0.10}_{-0.10}$	$1.15^{+0.09}_{-0.10}$	$0.8^{+0.1}_{-0.1}$	$7.8^{+0.4}_{-0.4}$	$56.89^{+0.05}_{-0.06}$
2015 May 11-C	FLWO	V	$0.996^{+0.002}_{-0.002}$	$4.4^{+0.7}_{-0.7}$						
2015 May 11-C	MINERVA/T3 and T4	Air	$0.999^{+0.002}_{-0.002}$	$4.0^{+0.7}_{-0.7}$						
2015 May 12-A	Perkins	R	$1.005^{+0.002}_{-0.002}$	$13.0^{+0.8}_{-0.8}$	$154.76274^{+0.00007}_{-0.00007}$	$0.79^{+0.14}_{-0.15}$	$1.23^{+0.20}_{-0.22}$	$1.6^{+0.4}_{-0.5}$	$6.1^{+0.7}_{-0.8}$	$2.05^{+0.09}_{-0.12}$
2015 May 12-A	MINERVA/T1 and T2	V	$1.000^{+0.005}_{-0.005}$	$12.0^{+1.5}_{-1.6}$						
2015 May 12-A	MINERVA/T3 and T4	Air	$1.000^{+0.005}_{-0.005}$	$15.5^{+1.8}_{-1.8}$						
2015 May 12-B	Perkins	R	$1.022^{+0.002}_{-0.002}$	$14.1^{+1.1}_{-1.3}$	$154.77076^{+0.00016}_{-0.00014}$	$0.16^{+0.08}_{-0.12}$	$2.62^{+0.32}_{-0.32}$	$14.0^{+5.8}_{-7.6}$	$8.3^{+1.0}_{-1.0}$	$2.82^{+0.08}_{-0.11}$
2015 May 12-B	MINERVA/T1 and T2	V	$1.010^{+0.004}_{-0.005}$	$11.8^{+1.5}_{-1.6}$						
2015 May 12-B	MINERVA/T3 and T4	Air	$1.006^{+0.005}_{-0.005}$	$10.4^{+1.7}_{-1.9}$						
2015 May 13-A	MINERVA/T1	R	$0.991^{+0.005}_{-0.005}$	$16.2^{+2.7}_{-2.7}$	$155.79517^{+0.00006}_{-0.00005}$	$0.33^{+0.06}_{-0.07}$	$1.03^{+0.13}_{-0.14}$	$3.1^{+0.8}_{-0.9}$	$4.1^{+0.4}_{-0.5}$	$1.45^{+0.05}_{-0.06}$
2015 May 13-A	Perkins	V	$1.007^{+0.003}_{-0.003}$	$25.1^{+1.4}_{-1.4}$						
2015 May 13-A	MINERVA/T4	Air	$0.996^{+0.006}_{-0.006}$	$25.6^{+3.2}_{-3.5}$						
				Individual Fits						
2015 May 13-B	Perkins	V	$1.017^{+0.005}_{-0.005}$	$15.9^{+3.1}_{-4.4}$	$155.81033^{+0.00010}_{-0.00011}$	$0.36^{+0.18}_{-0.26}$	$0.66^{+0.21}_{-0.22}$	$1.9^{+1.0}_{-1.5}$	$3.0^{+0.8}_{-1.0}$	$2.95^{+0.26}_{-0.42}$
2015 May 18	MINERVA/T4	Air	$0.998^{+0.007}_{-0.007}$	$32.8^{+4.6}_{-6.3}$	$160.66062^{+0.00010}_{-0.00010}$	$0.43^{+0.16}_{-0.16}$	$0.59^{+0.25}_{-0.25}$	$1.4^{+0.7}_{-1.1}$	$3.1^{+0.9}_{-0.9}$	$1.92^{+0.38}_{-0.52}$
				Individual Fits to Ground-Based Eclipses Presented by Vanderburg et al. (2015)						
2015 Mar 22	FLWO	V	$0.999^{+0.002}_{-0.002}$	$19.6^{+2.5}_{-3.3}$	$104.69519^{+0.00018}_{-0.00019}$	$1.61^{+0.20}_{-0.21}$	$0.21^{+0.11}_{-0.21}$	$0.1^{+0.1}_{-0.1}$	$5.5^{+0.7}_{-0.9}$	$6.16^{+0.07}_{-0.12}$
2015 Apr 11-A	FLWO	V	$1.023^{+0.001}_{-0.001}$	$56.5^{+1.2}_{-1.1}$	$123.66918^{+0.00003}_{-0.00003}$	$0.43^{+0.04}_{-0.04}$	$2.40^{+0.08}_{-0.08}$	$5.6^{+0.5}_{-0.6}$	$8.5^{+0.3}_{-0.3}$	$24.49^{+0.05}_{-0.09}$
2015 Apr 11-B	FLWO	V	$1.028^{+0.002}_{-0.001}$	$49.6^{+0.7}_{-0.8}$	$123.85688^{+0.00004}_{-0.00004}$	$1.20^{+0.07}_{-0.07}$	$2.07^{+0.10}_{-0.10}$	$1.7^{+0.2}_{-0.2}$	$9.8^{+0.3}_{-0.4}$	$8.34^{+0.05}_{-0.08}$
2015 Apr 17-A	MEarth	MEarth	$1.012^{+0.017}_{-0.017}$	$42.0^{+13.9}_{-16.3}$	$129.57600^{+0.00035}_{-0.00029}$	$0.98^{+0.47}_{-0.61}$	$0.85^{+0.41}_{-0.81}$	$0.8^{+0.6}_{-0.8}$	$5.5^{+1.9}_{-3.0}$	$0.28^{+0.02}_{-0.03}$
2015 Apr 17-B	MEarth	MEarth	$1.034^{+0.019}_{-0.020}$	$26.7^{+10.0}_{-10.4}$	$129.76344^{+0.00047}_{-0.00054}$	$1.39^{+0.81}_{-1.22}$	$1.93^{+0.95}_{-1.42}$	$1.3^{+1.0}_{-1.2}$	$10.0^{+3.8}_{-5.6}$	$0.52^{+0.02}_{-0.03}$
				Joint Fits to Ground-Based Eclipses Presented by Vanderburg et al. (2015)						
2015 Apr 18	MEarth	MEarth	$1.027^{+0.014}_{-0.015}$	$14.9^{+6.3}_{-7.3}$	$130.69954^{+0.00062}_{-0.00062}$	$2.41^{+1.36}_{-1.90}$	$1.73^{+0.88}_{-1.49}$	$0.7^{+0.4}_{-0.7}$	$12.4^{+4.9}_{-7.2}$	$0.24^{+0.02}_{-0.02}$
2015 Apr 18	MINERVA/T3	Air	$1.004^{+0.018}_{-0.023}$	$12.7^{+6.0}_{-7.0}$						

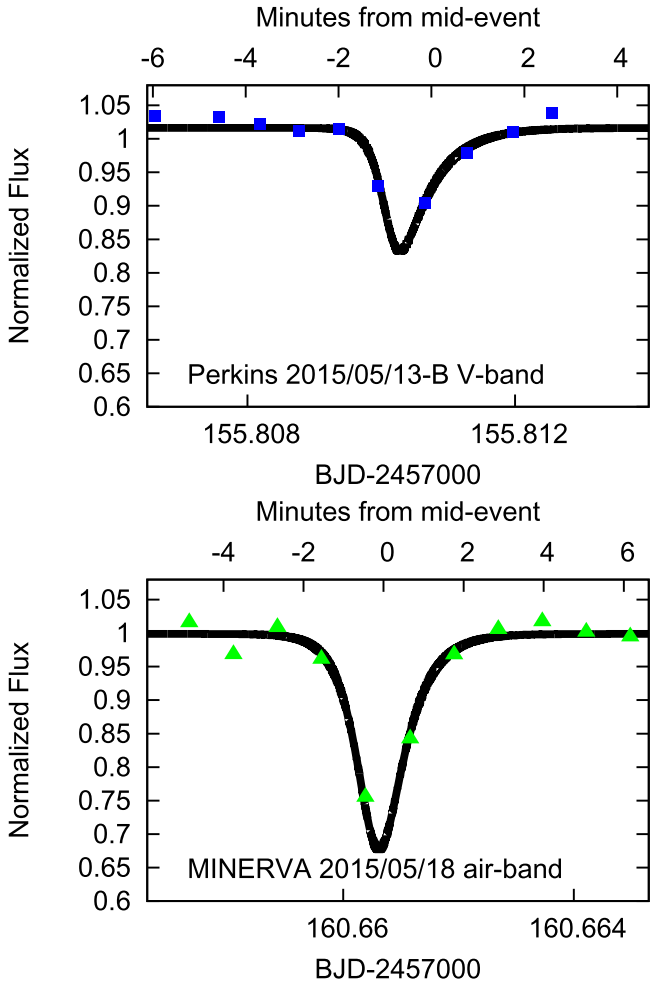

Figure 3. Asymmetric hyperbolic secant function fits to various significant flux drops of WD 1145+017, observed with a single telescope (from top to bottom, the Perkins and MINERVA telescopes, respectively).

3.3. Transit Profiles and a Limit on the Variability of the Ratio of Egress to Ingress Times

The weighted mean of the ratio of the egress to ingress times for all the ground-based transits in Table 2 is $\tau_2/\tau_1 = 0.73 \pm 0.06$. A constant egress to ingress time ratio model fits our eclipses with a reduced χ^2 of 11.8. Therefore there may be evidence of variations in the ratio of egress to ingress times. Although the weighted mean of the ratio of the egress to ingress times is just below unity, for most transits the egress lasts significantly longer than the ingress. For a few of our ground-based transits, the ingress seems to last marginally longer than the egress, and the errors on the ratio are smaller for these transits, leading to the weighted mean being near unity. In comparison, the median egress and ingress times from our ground-based transits are $\tau_1 = 0.79$ minute and $\tau_2 = 1.42$ minute, respectively, and the median ratio of the egress to ingress times is $\tau_2/\tau_1 = 1.73$, suggesting that indeed the egress typically lasts longer than the ingress.

We display the ratio of the egress to ingress times for the eclipse observed from the ground in the bottom panel of Figure 7. That the ingress is longer than the egress for at least some of our transits suggests the possibility of a leading cometary tail in addition to a trailing cometary tail for at least one or more of the planetesimals.

Our ground-based photometry also has sufficient precision that we are able to inspect the transit profiles of all the new eclipses we present in Table 2; the transits appear to be well fit by our asymmetric, hyperbolic secant (Equation (1)), suggesting that the transit profile is indeed very different than that of a solid transiting planet without a cometary tail passing in front of its host star.

3.4. A Limit on Single Size Grains in the Cometary Tails Trailing the Planetesimals around WD 1145+017

As the extinction efficiency generally increases with wavelength until the wavelength is comparable to the particle circumference (Hansen & Travis 1974), one can deduce the size of small dust grains from the wavelength dependence of their extinction. Although the wavelength, λ, differences in our current study between the V- ($\lambda \sim 0.55$ μm) and R-bands ($\lambda \sim 0.64$ μm) are small, the lack of wavelength-dependent transit depth differences in Table 3 allows us to rule out small dust grains. As the MINERVA "air" filter throughput is particularly wide, spanning near-ultraviolet to near-infrared wavelengths, we do not believe the ratio of our V or R to "air"-band observations will be particularly constraining on the particle sizes trailing the planetesimals around this white dwarf; we therefore do not use the "air"-band observations to attempt to place a particle size limit.

We employ the methodology we have already developed in Croll et al. (2014) to place a limit on the size of particles trailing the planetesimals orbiting WD 1145+017. We employ the Ångström exponent, $\alpha(a, \lambda_1, \lambda_2)$, a measure of the dependence of extinction on wavelength, defined as:

$$\alpha(a, \lambda_1, \lambda_2) \equiv -\frac{\log[\sigma_{\rm ext}(a, \lambda_2)/\sigma_{\rm ext}(a, \lambda_1)]}{\log(\lambda_2/\lambda_1)} \quad (4)$$

where λ_1 and λ_2 are the two wavelengths of interest, and a is the grain radius. The ratio of the transit depths, $D_{\lambda_2}/D_{\lambda_1}$, is approximately the ratio of the extinctions at these wavelengths: $\sigma_{\rm ext}(a, \lambda_2)/\sigma_{\rm ext}(a, \lambda_1)$. Therefore the ratio of the transit depths between the V- and the R-bands from Table 3 of $D_V/D_R = 0.96 \pm 0.17$ results in a ratio on the Ångström exponent of $\alpha(a, 0.55\ \mu\text{m}, 0.64\ \mu\text{m}) = 0.25$ with ranges -0.94 to 1.45 (1σ) and -2.14 to 2.64 (2σ).

We compare this limit to a Mie scattering calculation using the methodology discussed in Croll et al. (2014). We present the results, adapted to this white dwarf host, in Figure 8 assuming there is a single particle size in all the cometary tails in this system. We compare to hypothetical materials with a given index of refraction, n, and a complex index of refraction, k, as well as a number of materials that have previously been suggested to make-up the grains trailing disintegrating planets (Rappaport et al. 2012; Budaj 2013; Croll et al. 2014); these materials include pure iron, forsterite (Mg_2SiO_4; a silicate from the olivine family), enstatite ($MgSiO_3$; a pyroxene without iron), and corundum (Al_2O_3; a crystalline form of aluminum oxide). Using our transit depth ratio, materials with a typical index of refraction ($n \sim 1.6$) and a low complex index of refraction ($k < 0.01$; enstatite and forsterite satisfy these constraints at these wavelengths) single size particles must be at least $\sim$0.15 μm or larger, or $\sim$0.04 μm or smaller, with 2σ confidence. For corundum particles ($n \sim 1.6$ and $k < 0.04$ at these wavelengths), or other materials with similar indices of refraction, the limit on single size particles is $\sim$0.15 μm or

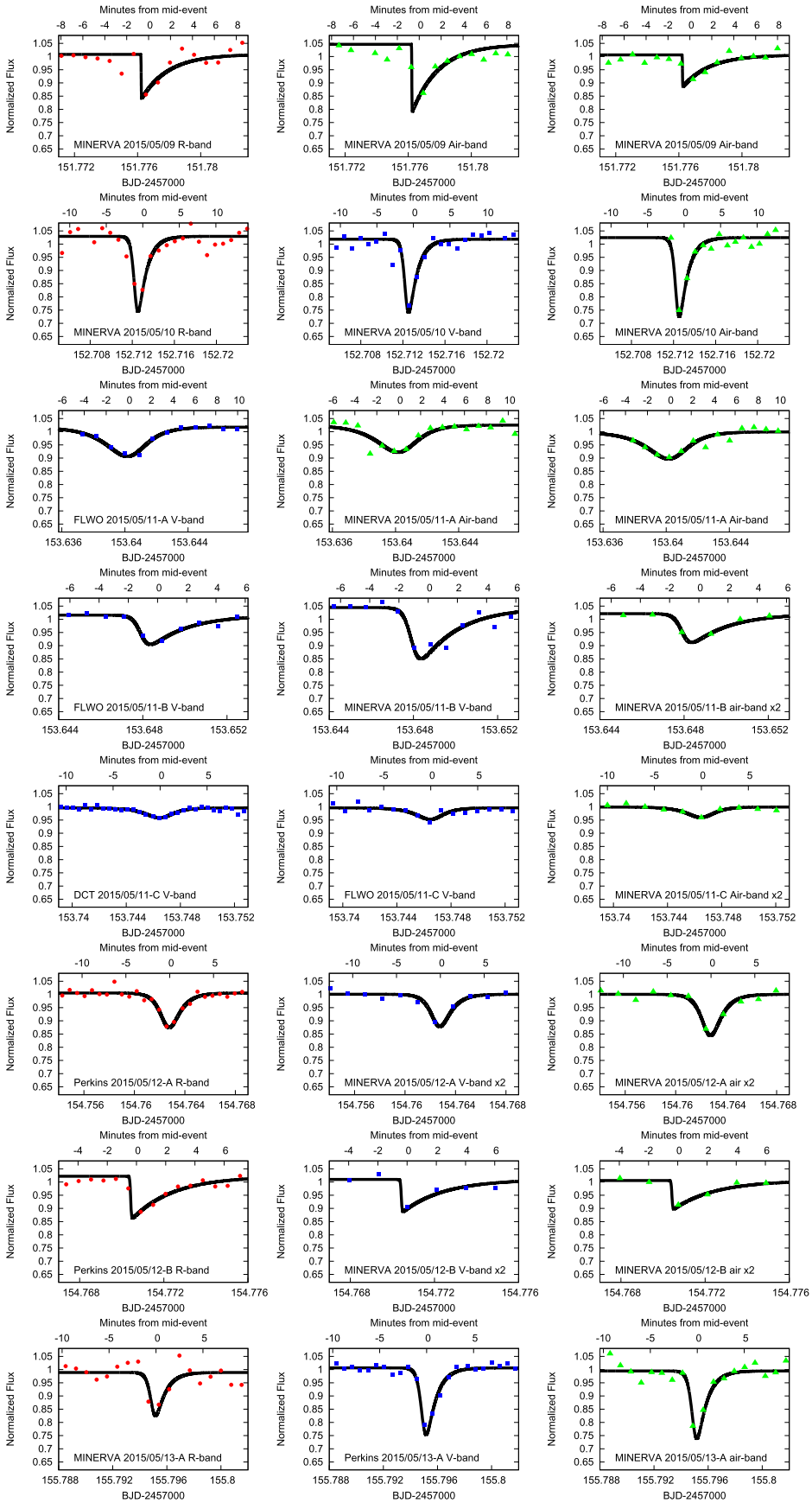

Figure 4. Asymmetric hyperbolic secant function fits to various significant flux drops of WD 1145+017, observed with the DCT, Perkins, FLWO, and MINERVA telescopes. Each row of observations in the plot occurs at the same time and is from different telescopes, often at a different wavelength, as indicated in the panels.

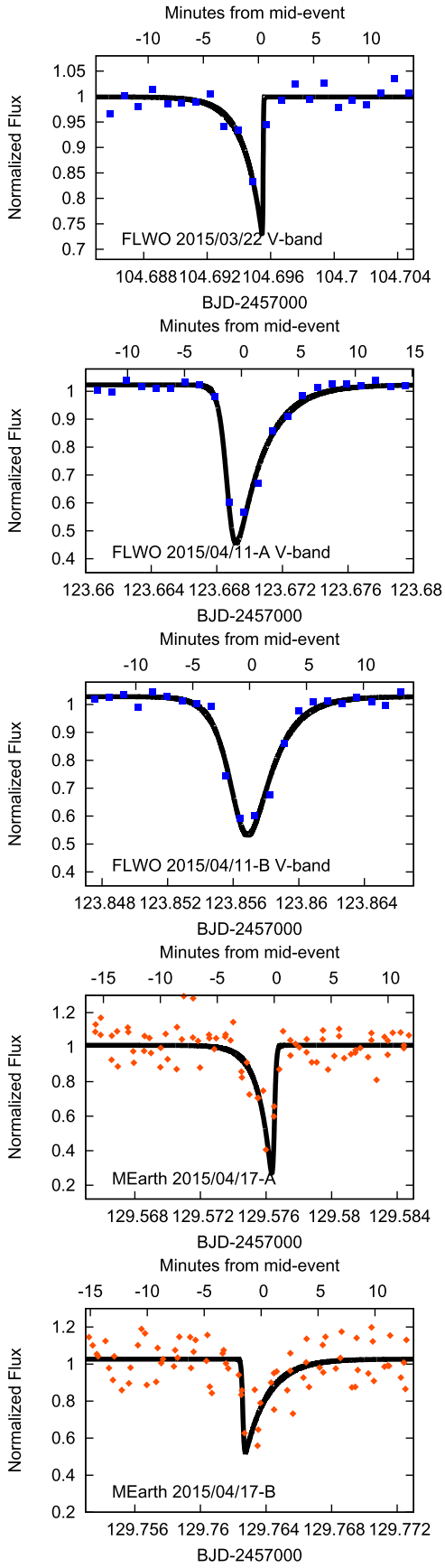

Figure 5. Asymmetric hyperbolic secant function fits to the significant flux drops of WD 1145+017 published previously by Vanderburg et al. (2015), and observed with the FLWO and MEarth telescopes.

larger, or ∼0.06 μm or smaller, with 2σ confidence. We cannot place a limit on pure iron particles, or on other materials with a high complex index of refraction ($k > 0.1$).

These limits prompt the question of whether such small iron, corundum, enstatite, and forsterite particles could survive for long enough to create the observed transits in the ∼1100 K environment (assuming the dust particles reradiate isotropically) at these short orbital periods around this white dwarf. The expected time for grains to travel the length of the cometary tail in this system (from Equation (6) of Rappaport et al. 2012, using the size of the occulting region, $R_o = 9.5\,R_\oplus$ from Section 3.2) is $\sim 1.6 \times 10^3$ s. Kimura et al. (2002) presents the sublimation lifetimes of various grains at various solar insolation levels. The stellar insolation of a dust grain in a ∼4.5 hr period around WD 1145+017 is equivalent to an orbit of 12 $R_\odot$ around our Sun (ignoring the difference in the shape of the stellar spectra); at these distances an amorphous olivine particle of size $a \sim 0.15$ μm survives for ∼100 s, while similar size crystalline olivines and pyroxenes survive for several orders of magnitude longer. Iron, which has a vapor pressure ∼50 times greater than that for olivines (Perez-Becker & Chiang 2013), and non-crystalline forsterite, seem unlikely to survive for the travel time required to create the observed transit durations. Orthoclase, albite, and fayalite were also mentioned by Vanderburg et al. (2015) as possible materials that might make up the cometary tails of these planetesimals; as they have similar or higher vapor pressures than iron, it seems unlikely that small particles of these materials could survive for long enough to create the observed transit durations. Crystalline forsterite, enstatite, and corundum of ∼0.15 μm or larger should survive for long enough without sublimating to travel the length of the occulting region. Generally, sublimation timescales, $t_{\rm sub}$, scale with the radius of the particle (Leberton et al. 2015), and therefore a related question is whether particles smaller than ∼0.15 μm are likely to survive the stellar insolation levels in this system for the required travel time. Even very small pyroxene particles, such as enstatite, should be able to survive these stellar insolation levels; it is less clear whether very small crystalline olivines, such as forsterite, are able to survive without sublimating. Given these arguments, henceforth we quote our limit on the radius of single-size particles in this system of ∼0.15 μm or larger, or ∼0.06 μm or smaller, with 2σ confidence, which applies to crystalline forsterite, enstatite, corundum, and materials with similar properties.

3.5. The Low-level Variability of WD 1145+017

Our photometry of WD 1145+017 also displays low-level variability; this low-level variability is best displayed in our 2015 May 11 and 18 DCT/LMI photometry of WD 1145+017 (Figure 9). On 2015 May 11 the variability we observe in our DCT light curve is generally consistent with the FLWO and MINERVA observations taken simultaneously.[13] For our 2015 May 11 photometry, even after excluding the data around the significant flux decrement at BJD-2457000 ∼ 153.74646 (we exclude data from BJD-2457000 = 153.735 to 153.750), the reduced χ^2 of our data compared to a flat line representing the mean normalized flux is ∼65, suggesting a flat line is an extremely poor fit to the data.

[13] On 2015 May 18 the MINERVA data obtained simultaneously is not of sufficient precision to make the statement that it is generally consistent (or inconsistent) with the DCT data obtained simultaneously.

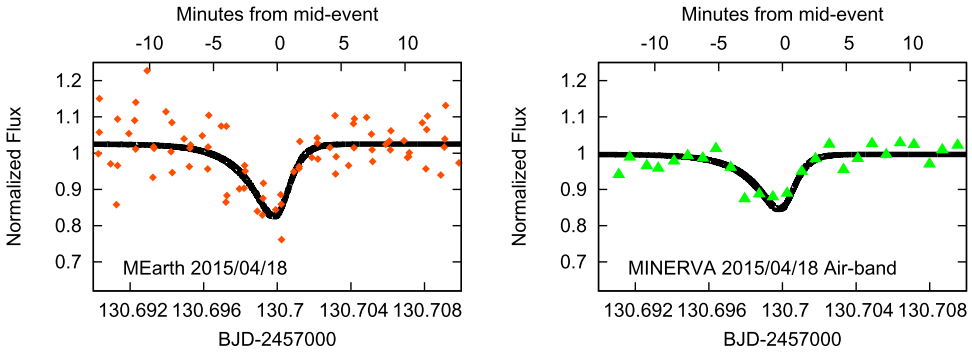

Figure 6. Asymmetric hyperbolic secant function fits to the flux drop of WD 1145+017 observed simultaneously on 2015 April 18 (UTC) with the MEarth and MINERVA/T3 telescopes. These data were published previously by Vanderburg et al. (2015), and the MINERVA/T3 data have been reanalyzed here.

Table 3
Joint "Transit Depth" Ratio Fits

Date (UTC) and Transit #	$T_{\rm min}$ (JD-2457000)	$D_{\rm air}/D_R$	D_V/D_R	$D_{\rm air}/D_V$
2015 May 09	$151.77662^{+0.00017}_{-0.00018}$	$0.65^{+0.21}_{-0.26}$, $1.39^{+0.27}_{-0.37}$	n/a	n/a
2015 May 10	$152.71259^{+0.00013}_{-0.00011}$	$1.05^{+0.19}_{-0.23}$	$1.01^{+0.16}_{-0.18}$	$1.04^{+0.16}_{-0.19}$
2015 May 11-A	$153.64016^{+0.00016}_{-0.00015}$	n/a	n/a	$0.95^{+0.12}_{-0.13}$, $0.91^{+0.14}_{-0.15}$
2015 May 11-B	$153.64838^{+0.00014}_{-0.00012}$	n/a	n/a	$1.74^{+0.24}_{-0.27}$, $0.97^{+0.15}_{-0.17}$
2015 May 11-C	$153.74646^{+0.00004}_{-0.00004}$	n/a	n/a	$1.17^{+0.19}_{-0.19}$, $1.04^{+0.20}_{-0.19}$
2015 May 12-A	$154.76274^{+0.00007}_{-0.00007}$	$1.19^{+0.14}_{-0.15}$	$0.93^{+0.12}_{-0.13}$	$1.29^{+0.20}_{-0.23}$
2015 May 12-B	$154.77076^{+0.00016}_{-0.00014}$	$0.73^{+0.13}_{-0.13}$	$0.83^{+0.11}_{-0.13}$	$0.87^{+0.17}_{-0.19}$
2015 May 13	$155.79517^{+0.00006}_{-0.00005}$	$1.58^{+0.26}_{-0.36}$	$1.55^{+0.22}_{-0.29}$	$1.02^{+0.13}_{-0.14}$
Weighted Mean	n/a	0.99 ± 0.24	0.96 ± 0.17	1.04 ± 0.24

This low-level variability we observe is not present in similarly faint reference stars, or with other blue reference stars in our field. For instance, if we reduce our reference star data in the same manner as for WD 1145+017 then the reduced χ^2 of four reference stars in the field that are similarly bright to WD 1145+017 (all four stars have V-magnitudes that are at most 0.5 mag brighter or 0.2 mag fainter than WD 1145+017) compared to flat lines representing the mean normalized flux of the reference star light curves are: 4, 5, 11, 14 (utilizing the same photometric errors that we use for WD 1145+017). For our reference-star light curves, there appears to be no significant, systematic deviations from a flat line; the deviations that exist appear to be consistent with white-noise. Thus, none of our reference-star light curves display the obvious systematic deviations that are present in the WD 1145+017 light curve. For this reason, the low-level variability we observe does not appear to be a systematic artifact, and is indeed intrinsic to WD 1145+017.

We do not attribute this low-level variability of WD 1145 +017 to pulsation, but instead due to dusty particles passing in front of the star along our line of sight, either due to the debris disk, or that have been ejected beyond the Roche lobe of one of the candidate planetesimals. The reason we do not attribute this variability to pulsation is that a white dwarf of the effective temperature ($T_{\rm eff} = 15{,}900 \pm 500$ K), surface gravity ($\log g$ ~8.0) and helium abundance (H/He $< 10^{-4.5}$) of WD 1145 +017 (Vanderburg et al. 2015) is not believed to pulsate; a white dwarf with these characteristics has not been observed to pulsate previously, and is not near a known white dwarf instability strip (Van Grootel et al. 2015).

3.6. Transit-timing Analysis

We perform a transit timing analysis using the $T_{\rm min}$ values from Table 2. The $T_{\rm min}$ values do not phase well with any one period and ephemeris, supporting the conclusion of Vanderburg et al. (2015) that there is more than one planetesimal transiting in front of the stellar host in this system. We notice that a number of our transits phase up with a ~4.5 hr period, and we display these results in Figure 10. Potentially up to three pairs of transits, one group of three transits, and one group of four transits, phase up with a ~4.5 hr period, but with different ephemerides. The group of four transits is the transits identified in Table 2 as 2015 May 09, 10, 11-B, and 12-B (the red points in Figure 10); these four transits phase up with a period $P = 4.4912 \pm 0.0004$ hr. We note that this is near the "A" period ($P = 4.49888 \pm 0.00007$ hr) from Vanderburg et al. (2015), but the errors indicate that these two periods are inconsistent with one another with strong confidence. The other pairs of transits that appear to phase up with a ~4.5 hr period include the pairs of ground-based transits observed on 2015 April 11 (A and B; the blue points in Figure 10 with an associated period of $P = 4.5048 \pm 0.0004$ hr), the 2015 May 11-A and 2015 May 12-A transits (the magenta points in Figure 10; $P = 4.4903 \pm 0.0007$ hr), and the 2015 May 13-A and 2015 May 18 transits (the orange points in Figure 10; $P = 4.4912 \pm 0.0002$ hr), while the group of three transits is the 2015 April 17 (A and B) and 2015 April 18 transits (the green points in Figure 10; $P = 4.494 \pm 0.003$ hr).

For the group of four transits (2015 May 09, 2015 May 10, 2015 May 11-B, and 2015 May 12-B), and the associated $P = 4.4912 \pm 0.0004$ hr orbit, on the subsequent night of observations (2015 May 13 UTC) and on several other

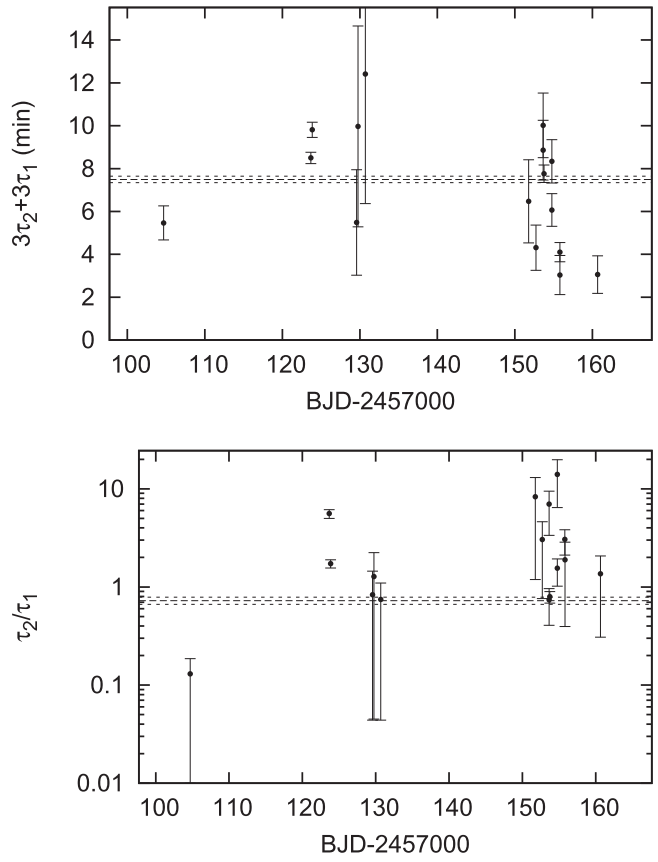

Figure 7. Constraints on the transit duration ($3\tau_1+3\tau_2$; top panel) and the ratio of the egress to ingress times (τ_2/τ_1; bottom panel) of the transits of WD 1145 +017 observed from the ground; in both panels the horizontal dashed line shows the weighted mean of the transit duration (top) and egress to ingress times (bottom), while the dotted line shows the 1σ uncertainty in these values. The transit duration and the ratio of the egress to ingress times display evidence that they may not be constant from eclipse to eclipse.

occasions, we have photometry that overlaps with a predicted transit for this period and ephemeris; no obvious deep transits (>10% of the stellar flux) are observed. Similarly, the ground-based photometry of Vanderburg et al. (2015) on 2015 April 17 displayed a pair of ∼40% deep transits separated by ∼4.5 hr that was followed by ∼15% transits on the following night. Given the variability that we observe in the depths and shapes for the transits on 2015 May 09, 10, 11-B, and 12-B, the lack of transits on subsequent nights, and the similar deep transits followed by much shallower transits displayed in the Vanderburg et al. (2015) ground-based photometry, this suggests that the dust tail trailing these candidate planetesimals evolves rapidly.

On the evenings of 2015 May 11 and 2015 May 12, the 2015 May 11-B and 2015 May 12-B transits come accompanied by another event that occurs approximately ∼12 minutes earlier; this event may occur on 2015 May 10 as well.

We have attempted to phase our ground-based eclipses with the periods and ephemerides of the A–F periods from Vanderburg et al. (2015) and include these in the bottom panel of Figure 10; our ground-based times are not obviously coincident with the predicted transit times from these periods and ephemerides, and therefore we cannot provide evidence in favor of the six specific periods and ephemerides given by Vanderburg et al. (2015). Arguably, this could have been foreseen as the durations of the events in the *K2* photometry are

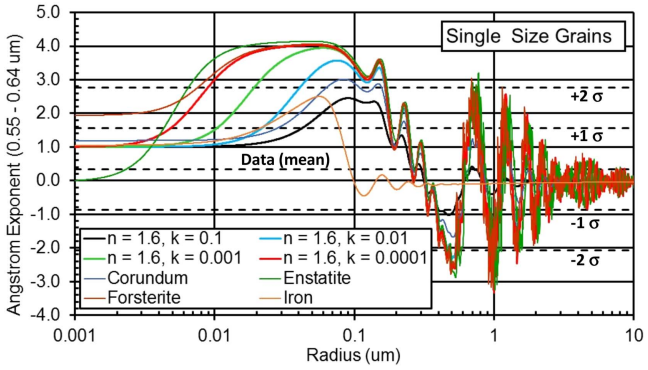

Figure 8. Plot of the Ångström exponent for spherical grains of a given radius for various materials, and for an index of refraction of $n = 1.6$ and for various imaginary components of the index of refraction, k. The horizontal dashed lines give the 1 and 2σ limits on the ratio of the transit depths, D, between our V- and R-band observations. Our limits on the Ångström exponent allow us to state that the radius of single sized grains in the dusty tails streaming behind these planetesimals must be ∼0.15 μm or larger, or ∼0.06 μm or smaller, with 2σ confidence.

generally inconsistent with the sharp, short-duration events that have been observed from the ground (Vanderburg et al. 2015). Our ground-based transits also do not phase with the predicted ephemerides from the ground-based MEarth and FLWO transits and the ∼4.5 hr period observed by Vanderburg et al. (2015).

We have also performed a blind period search to determine whether there are any other compelling periods for which a large fraction of the ground-based transit times phase up with a given period. To perform this search, we step through in frequency space in small frequency increments from periods of a few hours to a few days, and for each of the $T_{\rm min}$ values we predict future and past ephemerides using this tested period. We then determine the number of other $T_{\rm min}$ values that are close to the predicted ephemerides (we allow the $T_{\rm min}$ values to differ from the predicted ephemerides by at most 2% from the integer number of cycles of the tested period). No period other than the ∼4.5 hr period was particularly compelling.

Although period evolution (e.g., orbital decay) could reduce the number of planetesimals needed to explain the number and timing of the observed ground-based transits, nonetheless it appears that multiple planetesimals would still be required. Therefore, the timing of the eclipses we observe supports multiple planetesimals orbiting in close-period orbits around this white dwarf, but the exact number and periods of these bodies are unclear.

3.7. Analysis of the Persistence of the Six Periodic Transits in the K2 Photometry

Given the apparent rapid evolution of the depths and profiles of the transits in the ground-based photometry of WD 1145 +017, we reanalyzed the *K2* photometry of this system to determine whether the six claimed transiting bodies in this system persist in duration and depth throughout the 80 days of *K2* photometry. To do this, we split the *K2* photometry into three equal sections of ∼26.6 days; three equal 26.6 day sections were chosen as these sections were long enough in duration to allow for sufficient statistical accuracy, and short enough to allow for the evolution of these *K2* signals to be investigated. Reduction of the photometry was performed as discussed in Vanderburg et al. (2015). On each third of the *K2*

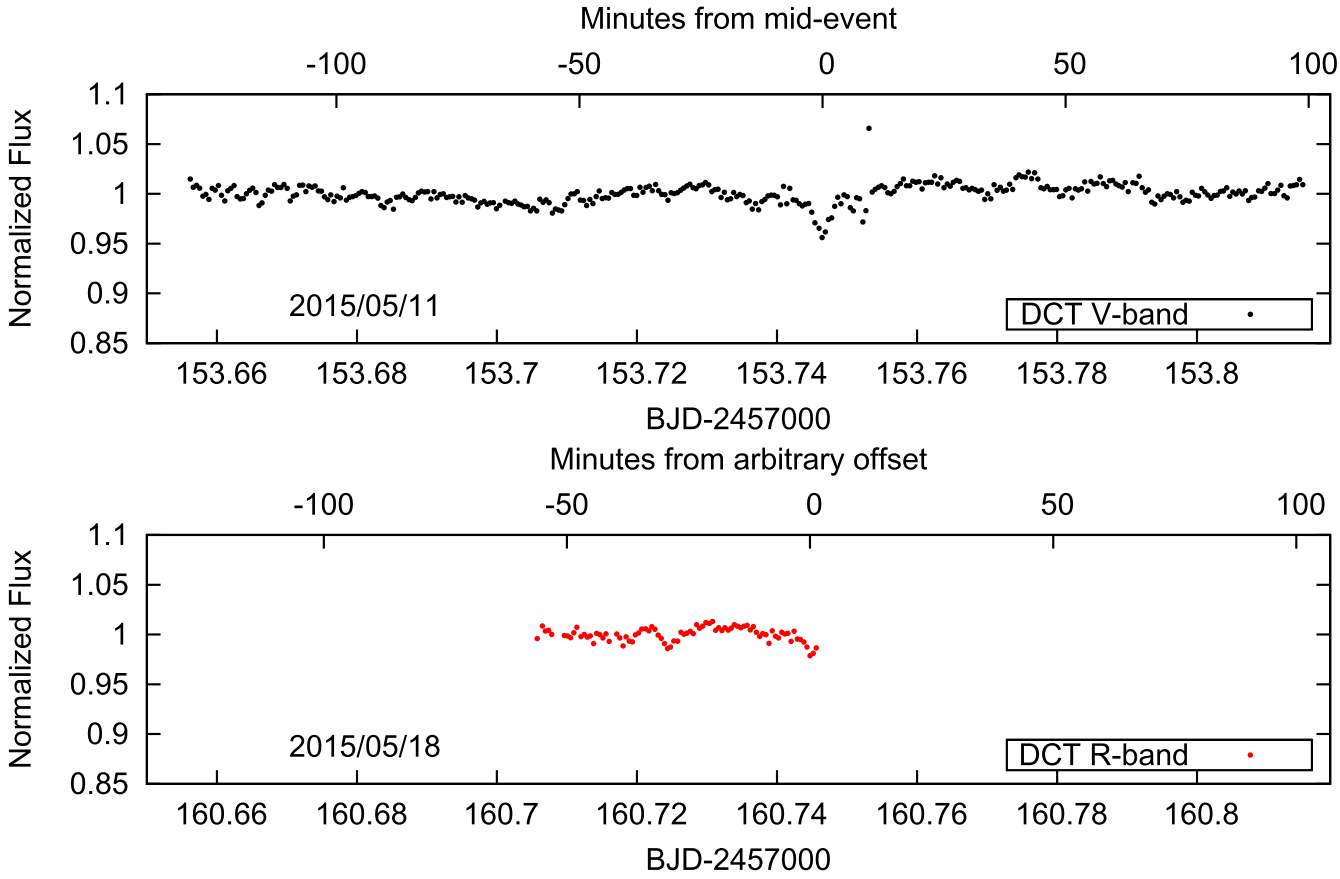

Figure 9. DCT/LMI observations of WD 1145+017 on UTC 2015 May 11 in the V-band (top) and on 2015 May 18 in the R-band (bottom). The observed low-level variability is unlikely to be due to pulsations, and is likely due to dusty material passing in front of the white dwarf and scattering light out of the line of sight.

photometry we perform a harmonic-summed Lomb–Scargle (LS) periodogram (Lomb 1976; Scargle 1982; Ransom et al. 2002), where the amplitudes from the first two harmonics are added to the fundamental frequency in the period range from 4 to 5 hr. We display these results, compared to the original LS periodogram signal from all the *K2* photometry, in Figure 11. We also phase the *K2* photometry to these periods, and present the phase binned transit signals in Figure 12. The transit dips at the original Vanderburg et al. (2015) A (∼4.499 day) and B (∼4.605 day) periods are present in all three thirds of the *K2* photometry, although they appear to vary in depth. The situation is less clear for the transits dips at the C (∼4.783 day), D (∼4.550 day), E (∼4.823 day), and F (∼4.858 day) periods. For the C, D, and F periods, in addition to varying in depth, it is unclear whether these signals exist in all three thirds of the *K2* photometry; for the C and D periods it is unclear whether the signal exists in the last third of *K2* photometry, while the F period is not clearly present in the first and second third of *K2* photometry. Although there appears to be a slight decrement at the transit mid-point in all three thirds of the *K2* photometry for the E period, the statistical significance of the E period detections in each third of *K2* photometry are not overwhelming. Therefore, one possibility is that this analysis indicates that the transits at the A–F periods simply evolve in depth over the 80 day of *K2* photometry; another possibility is that the transits at the C–F periods may not start to transit or may cease to transit for up to or more than ∼26 day of the 80 day of *K2* photometry.

4. Discussion and Conclusions

We have presented multiwavelength, multi-telescope, ground-based photometry of the white dwarf WD 1145+017 that revealed nine significant dips in flux of more than 10% of the stellar flux, and up to ∼30%. During our 2015 May observations we observe a transit with a depth greater than 10% of the stellar flux on average every ∼3.6 hr of observations, likely from more than one transiting body. Through fits to the transits that we observe, we confirm that the transit egress timescale is usually longer than the ingress timescale, and that the transit duration is longer than expected for a solid body at these short periods. All these lines of evidence support the conclusion of Vanderburg et al. (2015) that WD 1145+017 is likely orbited by multiple, low-mass planets/planetesimals in short-period orbits, likely with dusty cometary tails trailing behind them.

The exact number of planets/planetesimals orbiting WD 1145+017 and the periods of these objects is unclear. Given the substantial number of transit events that we observed, and that have been previously observed by Vanderburg et al. (2015), it seems likely that there are a number of planetesimals orbiting WD 1145+017. A number of our ground-based transits phase up well with a ∼4.5 hr period, however these events are best fit by drastically different ephemerides. Four of

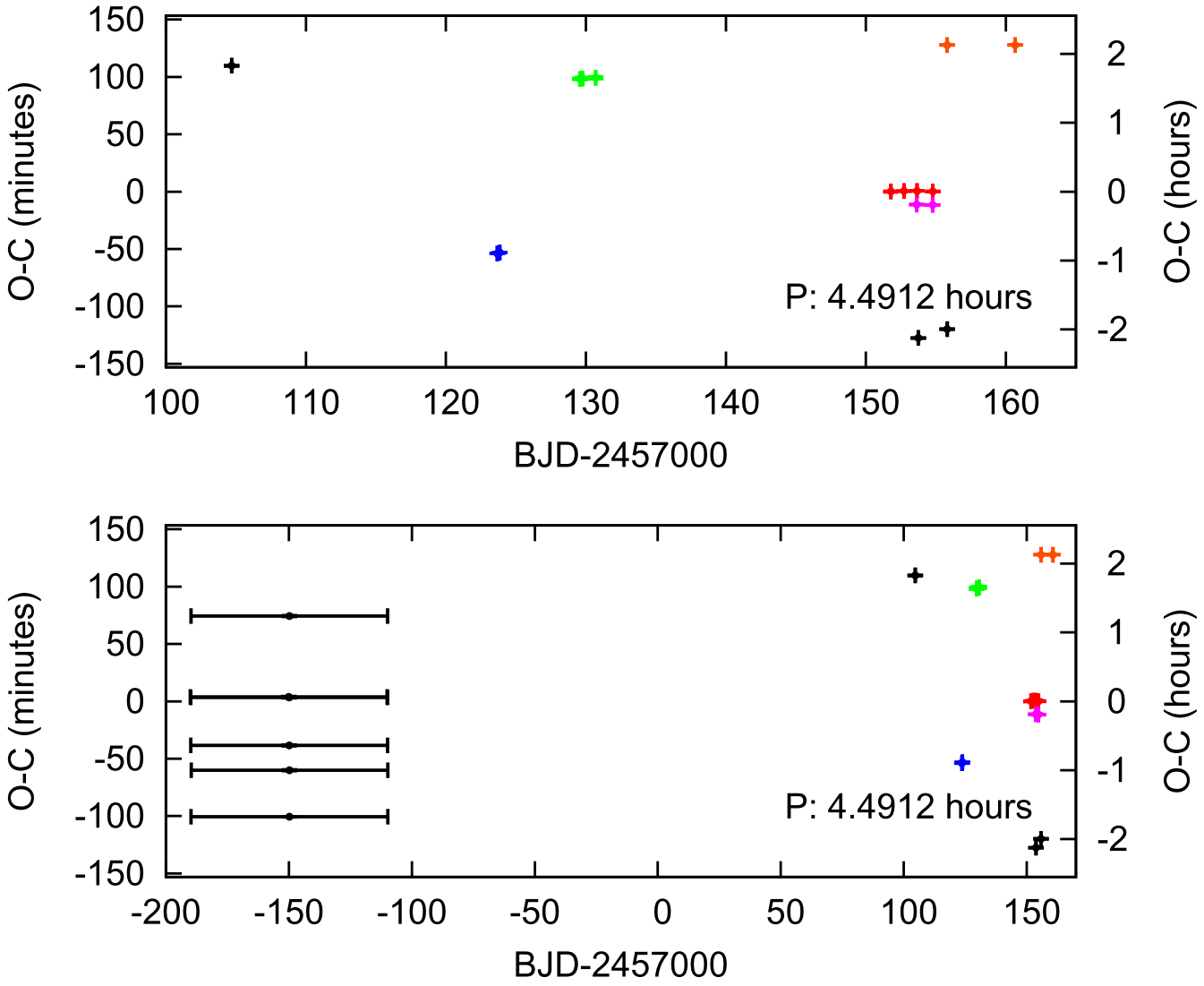

Figure 10. Transit-timing analysis (the black and colored points) phased to a period, $P = 4.4914$ hr, using the mid-transit times, $T_{\rm min}$, and associated errors from Table 2. The top panel features only the ground-based transit detections, while the bottom panel includes the six *K2* detections from Vanderburg et al. (2015). The x-error bars in the bottom panel signify that those data-points are averages over the ∼80 days of *K2* data. Multiple separate groups of transits (four transits denoted with red points, three transits denoted with green points, two transits denoted with with blue points, two transits denoted with magenta points, and two transits denoted with orange points) appear to phase with a ∼4.5 hr period, which is near the "A" period of Vanderburg et al. (2015).

our ground-based transit times are consistent with a constant ephemeris and a ∼4.5 hr period, but this ephemeris is not obviously consistent with the ephemerides of our other ground-based transits, the ground-based transit ephemerides of Vanderburg et al. (2015), or the *K2* periods and ephemerides of Vanderburg et al. (2015). This suggests that there are likely multiple objects in this system, and a number of these objects might have ∼4.5 hr orbital periods.[14]

We have also reanalyzed the *K2* photometry of this system to determine whether the signals for the six claimed transiting objects persist throughout the *K2* photometry. For four of the six claimed signals, the *K2* photometry is consistent with either depths that vary to nearly undetectable levels over the 80 days of *K2* photometry, or signals that may not transit or cease to transit during a significant fraction of the 80 days of *K2* photometry. This suggests that the amount of material in the cometary tails trailing these candidate planetesimals may evolve rapidly, or that we may be observing collisions, tidal break-up, or gravitational interactions that cause the orbits of these planetesimals to rapidly evolve.[15]

That we are unable to establish the rough number and the exact periods of the candidate planetesimals orbiting WD 1145 +017 has implications on the mass of these objects. The suggestion that the planetesimals orbiting WD 1145+017 might be approximately Ceres-mass ($\sim 1.6 \times 10^{-4}\, M_{\oplus}$) or less, came from an *N*-body simulation assuming six stable orbits with periods from ∼4.5–4.9 hr—such a collection of short-period objects with higher masses would quickly become unstable. Since we are unable to confirm the strict periodicity

[14] We note that while this manuscript was being revised, Gänsicke et al. (2016) and Rappaport et al. (2016) submitted manuscripts that made it much clearer that WD 1145+017 is orbited by up to 15 or more different transiting bodies, with different ephemerides; Rappaport et al. (2016) suggest this is due to multiple bodies being tidally ripped off a main asteroid in the system.

[15] While this manuscript was under revision, Rappaport et al. (2016) submitted a manuscript that argues that the many transiting bodies in the system are smaller fragmented pieces that are tidally broken off of a larger asteroid in the system.

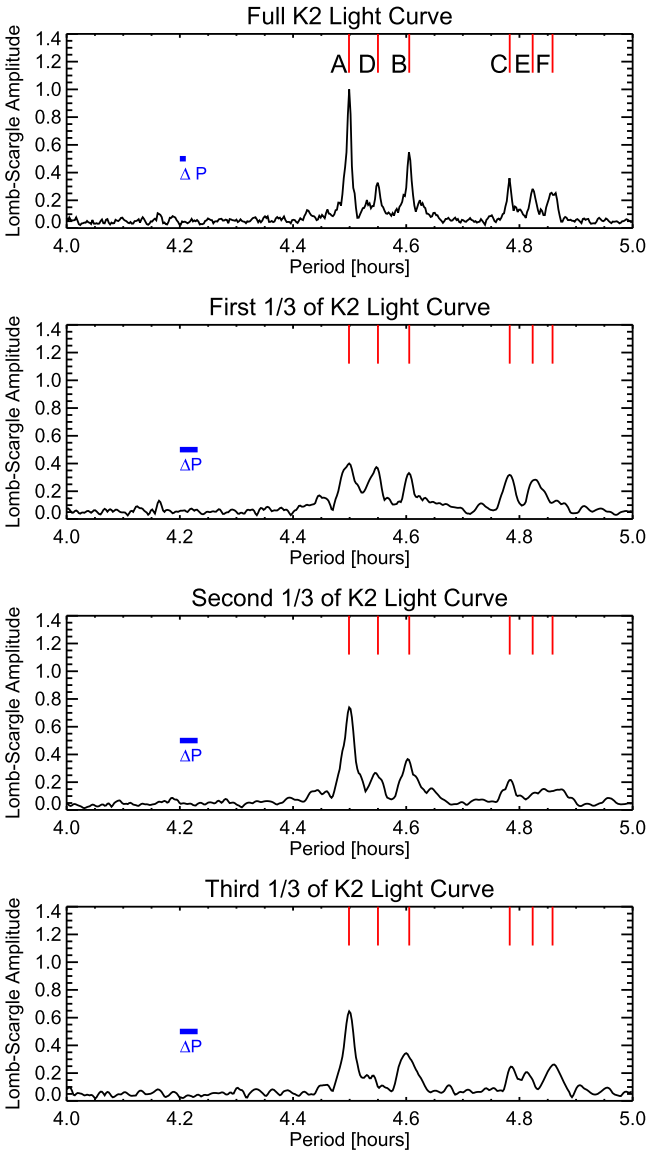

Figure 11. Summed Lomb–Scargle (LS) periodogram analysis of the *K2* photometry of WD 1145+017 (top panel), and the *K2* photometry split in three equal ∼26.6 day sections (bottom three panels). The vertical red dashes denote the A–F periods of Vanderburg et al. (2015). The horizontal blue line marked "ΔP" denotes the frequency resolution of the LS periodogram given by $\Delta P = 1/T$, where T is the duration of the photometry (80 day in the top panel, and ∼26.6 day in the bottom panels).

suggested by the *K2* photometry of this system, strict stability is not required by our observations and higher mass objects may be possible, including even planetary-mass objects;[16] such an orbital configuration is arguably unlikely, as a number of short-period, planet-mass objects would likely become unstable after a few million orbits or less (Vanderburg et al. 2015),[17] meaning that we would have to be observing this system during a unique epoch in its history.

The mechanism for the mass loss leading to the cometary tails that are believed to be trailing the candidate planetesimals in this system is also unclear. Our 2σ limit that the radius of single-size particles in the cometary tails streaming behind planetesimals in this system must be ∼0.15 μm or larger, or ∼0.06 μm or smaller, is consistent with a variety of scenarios.[18] If the objects in this system have a mass more typically associated with planets than planetesimals, then a Parker thermal wind may be required to lift material and escape the relatively strong surface gravity, similar to the other disintegrating planetary-mass candidates that have been presented thus far (Perez-Becker & Chiang 2013). If the objects in this system are planetesimal-mass objects—a more likely scenario since the orbits of such objects could be stable for a few million orbits or more—then in this lower surface gravity regime, the dusty material may escape the planetesimal via a number of mechanisms. For the first, analogous to comets in our own solar system (Cowan & A'Hearn 1979), vaporization of volatiles from the planetesimal's surface would drive dusty material from the surface. The second possibility is that the high temperature on the surface of the planetesimal would cause sublimation of rocky material into metal vapors. Under these high temperatures, the thermal speed of metal vapors would exceed the escape speed of the planetesimal; at altitude these vapors could condense into dusty material forming the observed cometary tails. Lastly, two other very different mechanisms may explain the candidate planetesimals and their cometary tails: collisions with other planetesimals in the system or with the debris disk, and tidal disruption of these planetesimals. For the collision scenario, if there are a number of planetesimals with short-period orbits that are embedded within, or nearby, the observed debris disk, collisions could lead to material trailing behind the planetesimals that would quickly shear to form tails (Veras et al. 2014); shear would also lead to cometary tails in a tidally disrupted body. Numerical simulations will have to be performed to determine whether such scenarios are consistent with the rapid night-to-night variability observed in both the transit depth and shape, including that deep transits are followed a night later by significantly shallower transits.[19]

Also, our highest precision photometry, obtained with the DCT, displays low amplitude variations. These variations are not believed to be due to pulsations from the white dwarf. Instead, this variability more likely suggests that dusty material consistently passes in front of the white dwarf. This observed material could be either from the detected debris disk in this system, or could be from material that has been ejected beyond the Roche lobe of the candidate planetesimals; either possibility could be consistent with the idea that these planetesimals are analogous to the Jupiter Ring–Moon system (Burns et al. 2004). If these lower amplitude events are periodic, due, for instance, to a number of smaller planetesimals in the system, then these lower amplitude variations could be responsible for the C–F periods from the *K2* photometry (Vanderburg et al. 2015).

[16] We note that observations of the WD 1145+017 system that were submitted while this manuscript was under revision suggest that the bodies orbiting this white dwarf are asteroid-mass, with the main body in the system having a mass about 1/10th the mass of Ceres (Rappaport et al. 2016).

[17] We also point the interested reader to the numerical simulations of Veras et al. (2016), which were submitted while this manuscript was being revised.

[18] We note that while this manuscript was under revision, Alonso et al. (2016) and Zhou et al. (2016) submitted manuscripts that placed even more stringent limits on the size of single-size particles in the cometary tails streaming behind objects in the WD 1145+017 system: the particles must be larger than ∼0.5 μm from four transits (Alonso et al. 2016) and larger than ∼0.8 μm from two transits of the WD 1145+017 system (Zhou et al. 2016).

[19] This statement assumes that these transits are associated with an object with a ∼4.5 hr period, that we have identified as the most likely for at least some of the planetesimals we have observed.

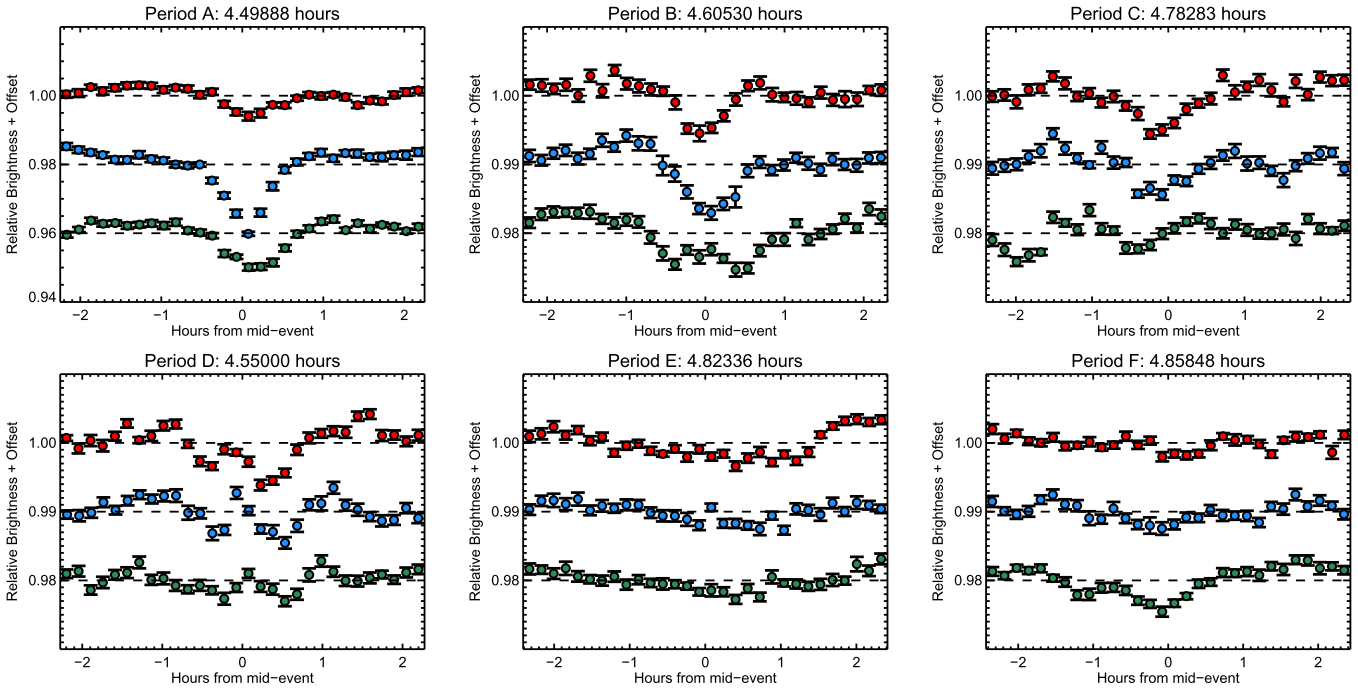

Figure 12. *K2* photometry of WD 1145+017 folded on the Vanderburg et al. (2015) A–F periods as indicated at the top of each panel. The red circles represent the first third (∼26.6 day) of the *K2* photometry, while the second and third ∼26.6 day stretches of *K2* photometry are represented by the blue and green circles, respectively. The data are binned every ∼0.033 in phase, and the various light curves are vertically offset for clarity.

That we are unable to determine the number of candidate planetesimals, and with the rapid transit-to-transit depth or profile evolution that we observe, suggests the possibility that rather than observing a planet or asteroid that has been disrupted, we may be observing a planet or asteroid in the midst of being tidal disrupted. Tidal disruption events have been previously suggested to endure for as short as a few years (Debes et al. 2012; Xu & Jura 2014). Therefore, follow-up observations over the next few years will determine whether the transit frequency, depths, and profiles are consistent with previous observing seasons, and whether there are a consistent number of orbiting objects in the system.[20]

Lastly, that we observe a significant transit dip (greater than 10% of the stellar flux) on average every ∼3.6 hr of observations, indicates that WD 1145+017 is a very favorable candidate for follow-up observations with larger telescopes. If this frequency of transit dips persists into the future then it is likely that a single night of observations of WD 1145+017 with larger ground-based or space-based telescopes will detect significant transit events, and reveal further information about this fascinating and confounding system.

We point the interested reader to the following manuscripts that present additional observations of this system and were submitted while this manuscript was being revised: Xu et al. (2016), Gänsicke et al. (2016), Rappaport et al. (2016), Alonso et al. (2016), Zhou et al. (2016), and Gary et al. (2016).

We thank the referee for a thorough review of this manuscript.

[20] Follow-up photometry that was performed while this manuscript was under revision during the Fall 2015 to Spring 2016 observing season (Gänsicke et al. 2016; Gary et al. 2016; Rappaport et al. 2016) suggests that there was a considerable increase in the number of transiting objects passing in front of WD 1145+017, and the depth of these transits, during that observing season, compared to the observations that we present here in Spring 2015.

These results made use of Lowell Observatory's Discovery Channel Telescope. Lowell operates the DCT in partnership with Boston University, Northern Arizona University, the University of Maryland, and the University of Toledo. Partial support of the DCT was provided by Discovery Communications. LMI was built by Lowell Observatory using funds from the National Science Foundation (AST-1005313).

MINERVA is a collaboration among the Harvard-Smithsonian Center for Astrophysics, The Pennsylvania State University, the University of Montana, and the University of New South Wales. It is supported with generous funds from the US NSF, NASA, and the Australian Research Council. MINERVA is made possible by generous contributions from its collaborating institutions and Mt. Cuba Astronomical Foundation, The David and Lucile Packard Foundation, National Aeronautics and Space Administration (EPSCOR grant NNX13AM97A), The Australian Research Council (LIEF grant LE140100050), and the National Science Foundation (grant 1516242). Any opinions, findings, and conclusions or recommendations expressed are those of the author and do not necessarily reflect the views of the National Science Foundation.

J.A.J. is supported by a generous grant from the David and Lucile Packard Foundation. The Center for Exoplanets and Habitable Worlds is supported by the Pennsylvania State University, the Eberly College of Science, and the Pennsylvania Space Grant Consortium.

We thank Dan Feldman and Connor Robinson for their assistance in observing this object with the Discovery Channel Telescope, Zachary Hall for his assistance with observing this object with the Perkins Telescope, Brian Taylor for his assistance in preparing observations of this object on both the Perkins and Discovery Channel Telescope, and Gilles Fontaine and Patrick Dufour for helpful conversations on white dwarf variability and pulsations.

References

Alonso, R., Rappaport, S., Deeg, H. J., & Palle, E. 2016, A&A, 589, 6
Bochinski, J. J., Haswell, C. A., Marsh, T. R., Dhillon, V. S., & Littlefair, S. P. 2015, ApJL, 800, L21
Budaj, J. 2013, A&A, 557, A72
Burns, J. A., Simonelli, D. P., Showalter, M. R., et al. 2004, in Jupiter: The Planet Satellites and Magnetosphere, ed. F. Bagenal et al. Vol. 1; Cambridge: Cambridge Univ. Press) 241
Carter, J. A., Winn, J. N., Holman, M. J., et al. 2011, ApJ, 730, 82
Cowan, J. J., & A'Hearn, M. F. 1979, M&P, 21, 155
Croll, B. 2006, PASP, 118, 1351
Croll, B., Albert, L., Jayawardhana, R., et al. 2015, ApJ, 802, 28
Croll, B., Rappaport, S., DeVore, J., et al. 2014, ApJ, 786, 100
Debes, J. H., & Sigurdsson, S. 2002, ApJ, 572, 556
Debes, J. H., Walsh, K. J., & Stark, C. 2012, ApJ, 747, 148
Dufour, P., Kilic, M., Fontaine, G., et al. 2010, ApJ, 719, 803
Dupuis, J., Fontaine, G., & Wesemael, F. 1993, ApJS, 87, 345
Eastman, J., Siverd, R., & Gaudi, B. S. 2010, PASP, 122, 935
Farihi, J., Gänsicke, B. T., & Koester, D. 2013, Sci, 342, 218
Gänsicke, B. T., Aungwerojwit, A., Marsh, T. R., et al. 2016, ApJL, 818, L7
Gary, B. L., Rappaport, S., Kaye, T. G., Alonso, R., & Hambschs, F. J. 2017, MNRAS, 465, 3267
Hansen, J. E., & Travis, L. D. 1974, SSRv, 16, 527
Howell, S. B., Sobeck, C., Haas, M., et al. 2014, PASP, 126, 398
Irwin, J. M., Berta-Thompson, Z. K., Charbonneau, D., et al. 2015, in 18th Cambridge Workshop on Cool Stars, Stellar Systems, and the Sun, ed. G. van Belle & H.C. Harris, 767
Janes, K. A., Clemens, D. P., Hayes-Gehrke, M. N., et al. 2004, BAAS, 36, 672
Jewitt, D., Agarwal, J., Weaver, H., Mutchler, M., & Larson, S. 2013, ApJL, 778, L21
Jewitt, D., Weaver, H., Agarwal, J., Mutchler, M., & Drahus, M. 2010, Natur, 467, 817
Jura, M. 2003, ApJL, 584, L91
Kimura, H., Mann, I., Biesecker, D. A., & Jessberger, E. K. 2002, Icar, 159, 529
Klein, B., Jura, M., Koester, D., Zuckerman, B., & Melis, C. 2010, ApJ, 709, 950
Koester, D., Gänsicke, B. T., & Farihi, J. 2014, A&A, 566, A34
Leberton, J., van Lieshout, R., Augereau, J.-C., et al. 2015, A&A, 555, A146
Lomb, N. R. 1976, Ap&SS, 39, 447
Massey, P., Dunham, E. W., Bida, T. A., et al. 2013, AAS, 221, #345.02
Michikami, T., Nakamura, A. M., Hirata, N., et al. 2008, EP&S, 60, 13
Nutzmann, P., & Charbonneau, D. 2008, PASP, 120, 317
Perez-Becker, D., & Chiang, E. 2013, MNRAS, 433, 2294
Raddi, R., Gänsicke, B. T., Koester, D., et al. 2015, MNRAS, 450, 2083
Ransom, S. M., Eikenberry, S. S., & Middleditch, J. 2002, AJ, 124, 1788
Rappaport, S., Barclay, T., DeVore, J., et al. 2014, ApJ, 784, 40
Rappaport, S., Gary, B. L., Kaye, T., et al. 2016, MNRAS, 458, 3904
Rappaport, S., Levine, A., Chiang, E., et al. 2012, ApJ, 752, 1
Sanchis-Ojeda, R., Rappaport, S., Pallè, E., et al. 2015, ApJ, 812, 112
Scargle, J. D. 1982, ApJ, 263, 835
Swift, J. J., Bottom, M., Johnson, J. A., et al. 2015, JATIS, 1, 2
Szentgyorgyi, A. H., Geary, J. G., Latham, D. W., et al. 2005, BAAS, 37, 1339
Vanderburg, A., Johnson, J. A., Rappaport, S., et al. 2015, Natur, 526, 546
Van Grootel, V., Fontaine, G., Brassard, P., & Dupret, M.-A. 2015, A&A, 575, A125
Veras, D., Leinhardt, Z. M., Bonsor, A., & Gänsicke, B. T. 2014, MNRAS, 445, 2244
Veras, D., Marsh, T. R., & Gänsicke, B. T. 2016, MNRAS, 461, 1413
Winn, J. N. 2010, arXiv:astro-ph/1001.2010
Xu, S., & Jura, M. 2014, ApJL, 792, L39
Xu, S., Jura, M., Dufour, P., & Zuckerman, B. 2016, ApJL, 816, L22
Zhou, G., Kedziora-Chudczer, L., Bailey, J., et al. 2016, MNRAS, 463, 4422
Zuckerman, B., Koester, D., Melis, C., Hansen, B. M., & Jura, M. 2007, ApJ, 671, 872
Zuckerman, B., Koester, D., Reid, I. N., & Hünsch, M. 2003, ApJ, 596, 477
Zuckerman, B., Melis, C., Klein, B., Koester, D., & Jura, M. 2010, ApJ, 722, 725